

4. G. H. Denton and W. Karlén, *Quat. Res.* **3**, 155 (1973).
5. L. D. D. Harvey, *Prog. Phys. Geogr.* **4**, 487 (1980).
6. J. M. Grove, *The Little Ice Age* (Methuen, London, 1988).
7. Error estimates in the dating of the GISP2 ice core are 2% for 0 to 11,640 years B.P. (2). For a more detailed description of dating methods used on the GISP2 ice core, see D. A. Meese *et al.*, "Preliminary depth-age scale of the GISP2 ice core," *Spec. CRREL Rep. 94-1* (Cold Regions Research and Engineering Laboratory, Hanover, NH, 1994). The time period 11,600 years B.P. corresponds to a core depth of ~1670 m.
8. Sampling and analysis of the core for glaciochemical species required specially adapted techniques to minimize contamination [P. A. Mayewski, M. J. Spencer, M. S. Twickler, S. Whitlow, *Ann. Glaciol.* **14**, 186 (1990); C. F. Buck *et al.*, *J. Chromatogr.* **594**, 225 (1992)].
9. In this model, sea salt components are estimated by an iterative process in which each sample is tested to determine which species is the most conservative (limiting). The limiting ion is then used to derive estimated sea salt concentrations, per sample, for the other species (3). This model assumes that no chemical fractionation occurred during sea salt aerosol formation and transport. Thus, if anything, it underestimates sea salt contributions to Summit snow and overestimates non-sea salt contributions. It is generally accepted that a limited fractionation, if any, of sea salt aerosols (excluding chloride) occurs [for example, R. A. Duce and E. J. Hoffman, *Annu. Rev. Earth Planet. Sci.* **4**, 187 (1976); E. J. Hoffman, G. L. Hoffman, I. S. Fletcher, R. A. Duce, *Atmos. Environ.* **11**, 373 (1977); E. J. Hoffman, G. L. Hoffman, R. A. Duce, *J. Geophys. Res.* **85**, 5499 (1980); D. L. Savoie and J. M. Prospero, *ibid.*, p. 385]. Estimated values of marine source species confirm that most of the Na (>99%) measured in the Holocene portion of the GISP2 core is derived from sea salt, whereas an estimated 73, 35, 19, 3, and 3% of Cl, Mg, K, Ca, and SO₄, respectively, are derived from sea salt. Sodium was used as the sea salt indicator for 4865 of the 5114 Holocene samples. Chlorine was used as the sea salt indicator for 233 of the samples, Mg for 10 samples, and K for 6 samples.
10. P. A. Mayewski *et al.*, *Science* **261**, 195 (1993).
11. J. P. Peixoto and A. H. Oort, *The Physics of Climate* (American Institute of Physics, New York, 1992).
12. L. D. Meeker, P. A. Mayewski, M. S. Twickler, S. I. Whitlow, in preparation.
13. M. Ters, in *Climate History, Periodicity, and Predictability*, M. R. Rampino, J. E. Sanders, W. S. Newman, L. K. Königsson, Eds. (Van Nostrand Reinhold, New York, 1987), pp. 205–237.
14. At the onset of the Holocene, sea level was about 40 m lower than it is today (13). Sea level is reported to have reached its modern position ~7000 to 8000 years B.P. along the U.S. [D. J. Cloquhoun and M. J. Brooks, in (13), pp. 143–156] and French Atlantic coasts (13). Little land ice was left for melting after ~7500 years B.P. [for example, G. H. Denton and T. J. Hughes, *The Last Great Ice Sheets* (Wiley, New York, 1981)].
15. N. Roberts and R. H. Wright, in *Global Climates Since the Last Glacial Maximum*, H. E. Wright *et al.*, Eds. (Univ. of Minnesota Press, Minneapolis, MN, 1993), pp. 194–220.
16. Results from the "Climates of the Holocene—Mapping Based on Pollen Data" (COHMAP) experiments.
17. J. E. Kutzbach and T. Webb III, in (15), pp. 5–11.
18. C. D. Charles, D. Rind, J. Jouzel, R. D. Koster, R. G. Fairbanks, *Science* **263**, 508 (1994).
19. H. H. Lamb, *Climate History and the Future* (Princeton Univ. Press, Princeton, NJ, 1977), vol. 2. The LIA is a term used widely to describe the cool period between the Middle Ages and the first half of the 20th century.
20. D. J. Erickson, J. T. Merrill, R. A. Duce, *J. Geophys. Res.* **91**, 1067 (1986); S. Whitlow, P. A. Mayewski, J. E. Dibb, *Atmos. Environ.* **A 26**, 2045 (1992); D. A. Mosher, P. Winkler, J. Jaffrezo, *ibid.* **27**, 2761 (1993).
21. R. E. Newell and Y. Zhu, *Geophys. Res. Lett.* **21**, 113 (1994).
22. J. F. O'Connor, *Mon. Weather Rev.* **89**, 211 (1961).
23. M. Stuiver and P. J. Reimer, *Radiocarbon* **35**, 215 (1993).
24. M. Stuiver and T. Braziunas, *Nature* **338**, 405 (1989).
25. J. R. Bray, *ibid.* **228**, 353 (1970); (3); D. A. Fisher, *Clim. Change* **4**, 419 (1982); W. Dansgaard, in *Climate Processes and Climate Sensitivity*, J. E. Harnness and T. Takahashi, Eds. (Geophysical Monograph, Washington, DC, 1984), vol. 29, pp. 288–298; V. C. LaMarche Jr., *Science* **183**, 1043 (1974).
26. C. P. Wake and P. A. Mayewski, *Tellus B* **46**, 220 (1994).
27. R. A. Berger and W. M. Berger, *The Global Water Cycle—Geochemistry and Environment* (Prentice Hall, Englewood Cliffs, NJ, 1987).
28. P. M. Grootes, M. Stuiver, J. W. White, S. Johnsen, J. Jouzel, *Nature* **366**, 552 (1993).
29. D. A. Meese *et al.*, *Science* **266**, 1680 (1994).
30. T. Blunier, J. Chappellaz, J. Schwander, B. Stauffer, D. Raynaud, *Nature* **374**, 46 (1995).
31. J. T. Andrews and J. D. Ives, in *Climate Changes During the Last 10,000 Years*, Y. Vasari, H. Hyvärinen, S. Hicks, Eds. (Univ. of Oulu, Oulu, Finland, 1972).
32. M. Stuiver, P. M. Grootes, T. F. Braziunas, *Quat. Res.*, in press.
33. P. A. Mayewski *et al.*, *J. Geophys. Res.* **98**, 12839 (1990).
34. A. L. Berger, *Quat. Res.* **9**, 139 (1978).
35. This work is a contribution to the Greenland Ice Sheet Project 2 (GISP2) and was supported by the NSF Office of Polar Programs. We thank our GISP2 and GRIP colleagues, E. Cook, and anonymous reviewers for their useful comments. We also thank the Polar Ice Coring Office (University of Alaska), the GISP2 Science Management Office (University of New Hampshire), and the 109th Air National Guard for their assistance.

13 June 1995; accepted 2 November 1995

Al Coordination Changes in High-Pressure Aluminosilicate Liquids

J. L. Yarger,* K. H. Smith, R. A. Nieman, J. Diefenbacher, G. H. Wolf, B. T. Poe, P. F. McMillan*

Understanding the effect of pressure on aluminosilicate glass and liquid structure is critical to understanding magma flow at depth. Aluminum coordination has been predicted by mineral phase analysis and molecular dynamic calculations to change with increasing pressure. Nuclear magnetic resonance studies of glasses quenched from high pressure provide clear evidence for an increase in the average coordination of Al with pressure.

Many igneous processes are influenced by the properties of molten aluminosilicates at depth (1). The variation in melt density with depth compared with that of the surrounding mantle will ultimately determine the buoyancy forces on the melts. Furthermore, the change in viscosity of the melt with pressure will determine the time scale for melt implantation, mineral crystallization and fractionation, and thermal transport. This has spurred a great deal of interest in understanding the thermodynamic and transport properties of aluminosilicate melts as a function of pressure and temperature.

Consisting of a fully polymerized tetrahedral network, SiO₂ has a high viscosity. Addition of a network modifier, such as Na₂O, breaks the Si–O–Si linkages to form Si–O[−]⋯Na⁺ [nonbridging oxygens (NBOs)] and lowers the viscosity. In contrast, the addition of Al₂O₃ to alkali-silicate melts (Na₂O:Al₂O₃ ≥ 1) removes the NBOs and reconstructs the tetrahedral network, increasing the viscosity. Aluminosilicate melts with a high silica content form three-dimensional tetrahedral networks

with extremely high viscosities. However, the viscosity of some highly silicic melts decreases with increasing pressure, so that their mobility at depth can be several orders of magnitude greater. A similar decrease in viscosity occurs in both natural and synthetic aluminosilicate melts, bracketing the entire composition range from andesitic to basaltic magmas (2). This anomalous behavior was first attributed to a pressure-induced increase in the Al coordination and a resultant weakening of the Al–O bond strength, analogous to that occurring in crystalline aluminosilicate minerals at high pressures (3). Subsequent spectroscopic experiments on glasses quenched from high-pressure melts showed no evidence of coordination change. Hence, the observed viscosity decrease was rationalized as bond weakening due to bond angle changes in the aluminosilicate tetrahedral network (4). An early report suggested evidence for six-coordinate Al in ambient albite (NaAlSi₃O₈) glasses quenched from melts formed at 6 and 8 GPa (5). This was later shown to be due to a trace of high-pressure crystalline material quenched into the glass samples. No definitive evidence has been found in subsequent work for high-coordinate Al sites in (high-silica) aluminosilicate glasses quenched from pressures up to 10 GPa (6).

Nuclear magnetic resonance (NMR) studies have revealed the presence of substantial amounts of high-coordinate Si (Si^{IV}

J. L. Yarger, K. H. Smith, R. A. Nieman, Department of Chemistry and Biochemistry, Arizona State University, Tempe, AZ 85287, USA.

J. Diefenbacher, G. H. Wolf, P. F. McMillan, Material Research Group in High-Pressure Synthesis, Arizona State University, Tempe AZ 85287, USA.

B. T. Poe, Bayerisches Geoinstitut, Universität Bayreuth, Bayreuth, Germany D-95440.

*To whom correspondence should be addressed.

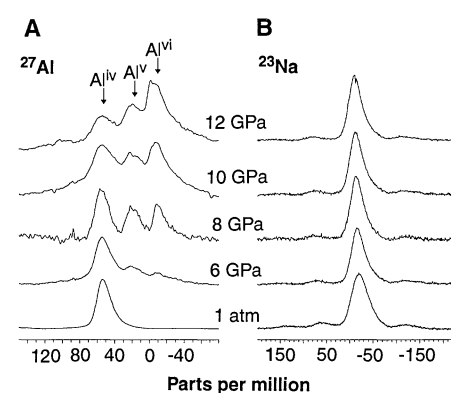
and Si^{IV}) species in partially depolymerized alkali silicate glasses quenched from high-pressure melts (7). These high-silica liquids exhibit a large viscosity decrease with increasing pressure, and the increase in Si coordination is proposed to play a key role in this change (7–10). High-coordinate Al species (Al^V and Al^{VI}) occur in high-temperature aluminosilicate liquids and quenched glasses at ambient pressure (11–13). However, these samples have metal oxide (M_nO_{n/2}):Al₂O₃ ratios < 1, and it would be expected from crystalline analogs that Al enters the network in sixfold coordination. Most natural melts have a higher ratio of metal oxide to Al₂O₃, and Al atoms enter the network in fourfold coordination (14). It is these liquids with which we are concerned. Any increase in the Al coordination with pressure would likely lead to a decrease in the high-pressure viscosity of these aluminosilicate melts. Although inferences based on in situ infrared spectroscopic studies at room temperature have been made for an increase in the Al coordination in aluminosilicate glasses (15), there has still been no definitive evidence for high-coordinate Al species in melts or glasses synthesized at high pressure. NMR spectroscopy of both the Al and Si coordination in glasses quenched from alkali-aluminosilicate liquids at high pressure provides unambiguous evidence that pressure drastically alters the Al coordination state in these liquids.

We investigated a model composition between albite [NaAlSi₃O₈ (Ab)] and sodium tetrasilicate [Na₂Si₄O₉ (NTS)]. We prepared 50:50 mole percent Ab:NTS glasses [Na₃AlSi₇O₁₇ (Ab₅₀NTS₅₀)] from melts at pressures between 6 and 12 GPa and at temperatures from 1900° to 2200°C in a multi-anvil device (16). The glasses obtained from quasi-isobaric quenches of the melts at high pressure were examined by ²⁷Al, ²⁹Si, and ²³Na magic angle spinning (MAS) NMR (17). In order to observe the weak ²⁹Si signal, we prepared one sample with 92% ²⁹Si-enriched material (18).

The ²⁷Al MAS NMR spectra (Fig. 1A) for the glasses prepared at high pressure clearly show three resonances that can be assigned to Al^{IV}, Al^V, and Al^{VI} species (11, 19, 20). In principle, the amount of each species is quantitatively determined from an integration of the peak areas. This modeling is complicated by the fact that the bands overlap and their precise form is not known. Although there is no unique means of modeling such multisite ²⁷Al spectra of glasses (21), a simple first-order model assumes that the asymmetric bandshape is the same for each species and is approximated by the band shape for the Al^{IV} site obtained in the spectrum of the ambient sample (given the same magnetic

field and spin rate). The fitting routine allows the width and amplitude to vary. This model allows for changes in the quadrupole coupling constants and quantity in each Al species. From these fits, the relative abundance of Al^{VI} markedly increases with pressure and is greatest for the sample at highest pressure (~48% at 12 GPa). In contrast, the amount of Al^V appears to go through a maximum (~28%) around 8 GPa (Table 1). These results may reflect the relative coordination distributions in the high-pressure samples; however, structural relaxation is known to occur on decompression in similar silicate glasses (10, 15).

The ²³Na MAS NMR (Fig. 1B) consists of a single broad resonance centered at -25 parts per million (ppm) relative to 1 M NaCl. ²³Na has a spin $I = 3/2$ and, like ²⁷Al ($I = 5/2$), suffers from quadrupole broadening. Because ²³Na has a smaller nuclear spin, for the same quadrupole coupling constant, Na has a larger second-order quadrupole breadth and hence broader lines. The lack of quadrupole splitting in the ²³Na resonance of Ab₅₀NTS₅₀ suggests a range of chemical shifts and quadrupolar coupling parameters, as expected for a disordered material (22). The pressure-quenched sam-



ples show a slight narrowing of the ²³Na resonance and a small shift in the peak position. The narrowing of linewidth is caused by a decrease in quadrupole coupling parameters or by a reduction in the range of chemical environments. Both effects can be interpreted as due to a slightly more symmetrical average coordination of Na at high pressure, but there is no evidence for a coordination change. The shift in peak position to increasing isotropic chemical shift (δ_{iso}) with pressure could indicate a slight shortening of the average Na–O bond distance (23).

In contrast to the behavior observed for Al, Si remains in tetrahedral coordination in the high-pressure (10 GPa) quenched sample. The ²⁹Si MAS NMR spectra of the glass sample prepared at 10 GPa is compared with that of an unpressurized ambient sample in Fig. 2. For both samples, the spectrum contains a single symmetric peak with a chemical shift consistent with Si sites that have four attached oxygens (Si^{IV}). The peak position for the 10-GPa sample is at -93.5 ± 0.4 ppm as compared with -95.1 ± 0.1 ppm for the unpressurized sample. The displacement to a less negative chemical shift in the high-pressure sample is consistent with a small decrease in the mean T–O–T bond angle

field and spin rate). The fitting routine allows the width and amplitude to vary. This model allows for changes in the quadrupole coupling constants and quantity in each Al species. From these fits, the relative abundance of Al^{VI} markedly increases with pressure and is greatest for the sample at highest pressure (~48% at 12 GPa). In contrast, the amount of Al^V appears to go through a maximum (~28%) around 8 GPa (Table 1). These results may reflect the relative coordination distributions in the high-pressure samples; however, structural relaxation is known to occur on decompression in similar silicate glasses (10, 15).

The ²³Na MAS NMR (Fig. 1B) consists of a single broad resonance centered at -25 parts per million (ppm) relative to 1 M NaCl. ²³Na has a spin $I = 3/2$ and, like ²⁷Al ($I = 5/2$), suffers from quadrupole broadening. Because ²³Na has a smaller nuclear spin, for the same quadrupole coupling constant, Na has a larger second-order quadrupole breadth and hence broader lines. The lack of quadrupole splitting in the ²³Na resonance of Ab₅₀NTS₅₀ suggests a range of chemical shifts and quadrupolar coupling parameters, as expected for a disordered material (22). The pressure-quenched sam-

Table 1. The abundance of Al^V and Al^{VI} in quenched glasses was estimated from the asymmetric peak areas of the $-1/2 \leftrightarrow 1/2$ (central transition) ²⁷Al NMR resonance. The δ_{iso} was estimated near the base of the asymmetric peaks. A convolution minimization fit to all three resonances in the spectra, allowing the amplitude and width to vary, gave a reasonable representation of the original spectra. Relative errors for the quantification of Al species were $\pm 6\%$.

Species	δ_{iso} (ppm)	Ab ₅₀ NTS ₅₀ integral (%)			
		6 GPa	8 GPa	10 GPa	12 GPa
AlO ₄ (Al ^{IV})	77	80	49	42	35
AlO ₅ (Al ^V)	40	12	28	20	17
AlO ₆ (Al ^{VI})	8	8	23	38	48

found to occur in densified silicate glasses (24). Within detection limits, there is no indication of any Si^{V} or Si^{VI} , which would show resonances near -150 and -200 ppm, respectively (7, 25).

The quench rates used in the preparation of the glasses in this study are similar to those used in previous high-pressure studies of alkali-silicate glasses (6, 7). In the studies of alkali-silicate glasses, Si occurred in high-coordinate sites in samples quenched from 10 GPa. The experimental results shown here indicate that the coordination increase occurs preferentially on the Al sites when both Si and Al are present. Furthermore, our results are quite different from that previously reported for Ab glass prepared at high pressure (6). For the albite composition, which has a fully polymerized tetrahedral network, both Al and Si occurred in tetrahedral coordination in samples quenched from 10 GPa. Our work further underscores previous suggestions that NBOs provide a low-energy pathway for pressure-induced coordination changes of the network-forming cations (7, 10, 26).

Recent studies indicate that viscous flow in alkali-aluminosilicate liquids is constrained by oxygen exchange between polymeric units (8, 12, 20, 23, 27). In this model of viscous flow, the structural relaxation occurs through formation of transient five-coordinated (Si^{V} or Al^{V}) species. Increasing pressure favors formation of the high-coordinate species and, consequently, lowers the activation energy (E_a) for oxygen exchange. The viscosity can also be lowered in the pressure range of the coordination change by an increase in the number of isoergic configuration states in the melt, thus increasing the number of channels available for stress relaxation (9, 28). Both of these contributions to the pressure-induced reduction in the viscosity of alkali aluminosilicate liquids are incorporated in the Adam-Gibbs expression for cooperative relaxation in polymer melts (28), which leads to the following expression for shear viscosity (η):

$$\eta = \eta_0 \exp(-C/TS_c) \quad (1)$$

where T is the temperature, C is related to the activation energy barrier for relaxation, and S_c is the configurational entropy of the melt. For binary silicates, viscous flow in pure silica (SiO_2) requires breaking strong Si-O bonds (452 kJ/mol), leading to a high viscosity (26). Adding alkali creates NBOs, which lowers the barrier for formation of high-coordinate network cations, in turn reducing viscosity. As one adds Al_2O_3 , the NBO concentration is decreased, the activation energy increases, and the viscosity increases (26). However, an increase of pressure forms high-coordinate Al and the viscosity decreases strongly. As the composition approaches that of albite ($M_n\text{O}_{n/2}:\text{Al}_2\text{O}_3 = 1$), the number of NBOs becomes negligible, and the Al^{V} intermediate must be created through a bridging oxygen. This requires a higher activation energy, which explains the maximum in viscosity along the fully polymerized alkali-aluminosilicate join with $\text{Na}_2\text{O}:\text{Al}_2\text{O}_3 = 1$ and the lack of high-coordinate cations upon quenching (6, 26). This inability to quench a high-coordinate cation is also observed in other fully polymerized tetrahedral networks such as SiO_2 and GeO_2 (15, 29). The framework cations in these tetrahedral glasses are known to go through a transition to six-coordinate; however, upon decompression the glass reverts to a tetrahedral coordination. By departing in composition from the fully polymerized $\text{Na}_2\text{O}:\text{Al}_2\text{O}_3$ join to create NBOs, high-coordinate Al species can be quenched from high pressure, as shown in Fig. 1.

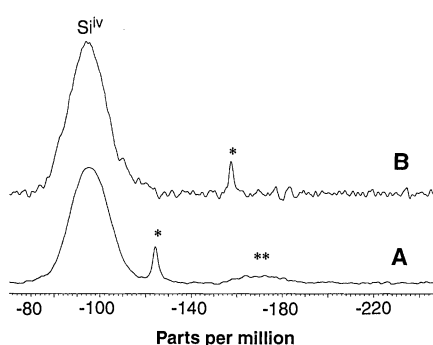
The presence of high-coordination Al in high-pressure aluminosilicate liquids at depth has been a controversial issue in geochemistry. Recent MAS NMR spectra and molecular dynamic simulations have shown that both Al^{V} and Al^{VI} likely exist in high-temperature aluminosilicate ($M_2\text{O}-\text{Al}_2\text{O}_3-\text{SiO}_2$) liquids (12, 13, 20). We have now shown that pressure also increases the Al coordination in alkali-aluminosilicate glasses. It is interesting

that Al is strongly preferred over Si for high-coordinate sites in aluminosilicate glasses at high pressure. Thus, a pressure-induced Al coordination change is likely to be a much more important mechanism in influencing the properties of natural magmas in the Earth's upper mantle (<300 km) than are Si coordination changes. Our data suggest that a large viscosity decrease with pressure should be observed for liquids at this composition (2, 30), which provides a model for natural basalt to andesitic magmas. Further, the apparent maximum in the concentration of Al^{V} species in the glass quenched from 8 GPa might indicate a change in the rate of decrease in viscosity near this pressure (30).

REFERENCES AND NOTES

1. A. E. Ringwood, *Chem. Geol.* **82**, 187 (1990).
2. I. Kushiro, *Earth Planet. Sci. Lett.* **41**, 87 (1978); *J. Geophys. Res.* **81**, 6347 (1976); _____, H. S. Yoder, B. O. Mysen, *ibid.*, p. 6351.
3. H. S. Waff, *Geophys. Res. Lett.* **2**, 193 (1975).
4. S. K. Sharma, D. Virgo, B. O. Mysen, *Am. Mineral.* **64**, 779 (1979); P. F. McMillan and C. Graham, *Progress in Experimental Petrology*, C. Ford, Ed. (Natural Environment Research Council Publ. Series D18, Eaton, Manchester, UK, 1981), pp. 113-116; B. O. Mysen, D. Virgo, P. Danckwerth, F. A. Seifert, I. Kushiro, *Neves Jahrb. Mineral. Abh.* **147**, 281 (1983).
5. E. Ohtani, F. Taulelle, C. A. Angell, *Nature* **314**, 78 (1985).
6. J. F. Stebbins and D. Sykes, *Am. Mineral.* **75**, 943 (1990); D. Sykes, B. T. Poe, P. F. McMillan, R. W. Luth, R. K. Sato, *Geochim. Cosmochim. Acta* **57**, 1753 (1993).
7. X. Xue, J. F. Stebbins, M. Kanzaki, R. Trönnnes, *Science* **245**, 962 (1989); J. F. Stebbins and P. F. McMillan, *Am. Mineral.* **74**, 965 (1989); X. Xue, J. F. Stebbins, M. Kanzaki, P. F. McMillan, B. Poe, *ibid.* **76**, 8 (1991).
8. J. F. Stebbins, *Nature* **351**, 638 (1991); _____, I. Farnan, X. Xue, *Chem. Geol.* **96**, 371 (1992); J. F. Stebbins and P. F. McMillan, *J. Non-Cryst. Solids* **160**, 116 (1993).
9. J. E. Dickinson, C. M. Scarfe, P. McMillan, *J. Geophys. Res.* **B95**, 15675 (1990).
10. G. H. Wolf, D. J. Durben, P. F. McMillan, *J. Chem. Phys.* **93**, 2280 (1990).
11. S. H. Risbud, R. J. Kirkpatrick, A. P. Tagliavere, B. Montez, *J. Am. Ceram. Soc.* **70**, C10 (1987); R. K. Sato, P. F. McMillan, P. Dennison, R. Dupree, *J. Phys. Chem.* **95**, 4483 (1991).
12. B. Poe, P. F. McMillan, B. Coté, D. Massiot, J. P. Coutures, *J. Phys. Chem.* **96**, 8220 (1992).
13. _____, *Science* **259**, 786 (1993).
14. B. O. Mysen, *J. Geophys. Res.* **95**, 15733 (1990).
15. Q. Williams and R. Jeanloz, *Science* **239**, 902 (1988).
16. A 1200-ton Sumitomo uniaxial split-sphere multi-anvil apparatus at the University of Bayreuth in Germany was used to obtain pressure in the $\text{Ab}_{50}\text{NTS}_{50}$ quench experiments. The sample assembly consisted of a MgO octahedron with a lanthanum chromite (LaCrO_3) cylindrical heater around a platinum-enclosed sample. Toshiba F-grade WC anvils with edge lengths of 2 to 4 mm were used for pressure generation [A. R. Remsberg, J. N. Boland, T. Gasparik, R. C. Liebermann, *Phys. Chem. Minerals* **15**, 498 (1988)]. Pressure was calibrated at room temperature with the use of transitions in Bi. Also, calibrations at 1000° and 1450°C were done by reversal of the equilibria of quartz \leftrightarrow coesite, coesite \leftrightarrow stishovite, and Fe_2SiO_4 olivine \leftrightarrow spinel transitions [D. C. Rubie, C. R. Ross II, M. R. Carroll, S. C. Elphick, *Am. Mineral.* **78**, 574 (1993)]. Samples were first compressed, then heated to a temperature of

Fig. 2. The ^{29}Si NMR of labeled $\text{Ab}_{50}\text{NTS}_{50}$ thermally quenched from the liquid state at two different pressures to obtain glasses under the same conditions as the samples used in the Al and Na NMR analysis. The 1-bar-pressure quenched glass (A) and the 10-GPa quenched glass (B) were loaded into a Si_3N_4 rotor (*) for MAS NMR at a spin rate of 6.0 ± 0.002 kHz and 8.6 ± 0.002 kHz, respectively. The only resonance observable in either spectrum is that of a four-coordinate silicon (Si^{IV}) and its spinning sidebands (**). Differing spinning speeds were tested to ensure that the rotor and Si^{IV} sidebands were not masking any high-coordinate resonance. The spectra are internally referenced to the Si_3N_4 rotor (-48.8 ppm relative to tetramethylsilane). The MAS NMR spectra were obtained under different spinning rates to ensure that neither the rotor nor the sample sidebands were masking any high-coordinate resonances.



- 1800° to 2000°C. The samples stayed at that temperature for 10 to 20 min before being quenched by the cutting off of power to the furnace. The quench rate was measured to be ~500°C per second. The samples were subsequently decompressed at a rate of 2 to 3 GPa/hour.
17. NMR spectra described here were collected with a Varian Unity spectrometer operating at 9.4 T was a MAS probe from Doty Scientific (Columbia, SC), with 3.5-mm rotors commonly spinning at 9.3 kHz (unless otherwise specified). To make ^{27}Al analysis as straightforward as possible, a small tip angle ($< \pi/6$) was used in all cases. ^{23}Na and ^{27}Al NMR was done with the use of delay times on the order of 1 s, with a spectral band width of 2 MHz. For ^{29}Si NMR, a smaller spectral band width was used because of the limited chemical shift range in Si; however, much longer delay times were used (70 s) because of the possibility of having long relaxation times for Si species even with a small paramagnetic dopant (Gd_2O_3) [A. Abragam, *Principles of Nuclear Magnetism* (Oxford Univ. Press, New York, 1961)]. We subtracted a ^{27}Al background from the probe by collecting data on an empty rotor under conditions identical to those under which the glass samples were run. There was no probe background in the ^{23}Na and ^{29}Si spectra; however, the Si_3N_4 rotors gave a characteristic resonance at -48.8 ppm relative to tetramethyl silane at 0 ppm with spinning sidebands in the silicon NMR. This was used as an internal chemical shift calibration for ^{29}Si NMR. To reference the chemical shift of ^{23}Na and ^{27}Al , a liquid sample of 1 M NaCl (0 ppm) and 1 M AlCl_3 (0 ppm) was run before each spectrum, respectively.
18. We prepared the ^{29}Si -enriched $\text{Ab}_{50}\text{NTS}_{50}$ by fusing stoichiometric amounts of 92%-labeled $^{29}\text{SiO}_2$ glass (Cambridge Isotope Laboratory, Andover, MA) with sodium carbonate (Na_2CO_3), aluminum oxide (Al_2O_3), and 0.1 weight percent gadolinium oxide (Gd_2O_3) at 1200°C for 2 hours. Glass was formed upon removal of the Pt crucible containing the mixed liquid components from the furnace. We did not chemically analyze the sample because of the expense of labeled material and the proven nature of the synthesis process. Gd_2O_3 was added to shorten the spin-lattice relaxation time of Si. This sample, along with unlabeled glass made under the same conditions, was then sealed in Pt capsules for use in the high-pressure multi-anvil quenching described in (16).
19. C. Jäger, G. Kunath, P. Losso, G. Scheler, *Solid State NMR* **2**, 73 (1993).
20. B. T. Poe, P. F. McMillan, B. Coté, D. Massiot, J. Coutures, *J. Am. Ceram. Soc.* **77**, 1832 (1994).
21. A. Samoson, *Chem. Phys. Lett.* **119**, 29 (1985); D. Massiot, B. Coté, F. Taulelle, J. P. Coutures, *Application of NMR Spectroscopy to Cement Science* (Gordon and Breach Science, Tokyo, Japan, 1994), pp. 153–170; G. Kunath-Fandrei, T. J. Bastow, C. Jäger, M. E. Smith, *Chem. Phys. Lett.* **234**, 431 (1995).
22. R. J. Kirkpatrick, R. A. Kinsey, K. A. Smith, K. M. Henderson, E. Oldfield, *Am. Mineral.* **70**, 106 (1985).
23. J. F. Stebbins and I. Farnan, *Science* **255**, 586 (1992); X. Xue and J. F. Stebbins, *Phys. Chem. Minerals* **20**, 297 (1993); C. Schmelz and J. Stebbins, *Geochim. Cosmochim. Acta* **57**, 3949 (1993); P. Fiske and J. Stebbins, *Am. Mineral.* **79**, 848 (1994).
24. R. A. B. Devine, R. Dupree, I. Farnan, J. J. Capponi, *Phys. Rev. B* **35**, 2560 (1987).
25. R. Dupree, D. Holland, M. Mortuza, *Nature* **328**, 416 (1987).
26. P. F. McMillan, B. T. Poe, P. Gillet, B. Reynard, *Geochim. Cosmochim. Acta* **57**, 3653 (1994).
27. I. Farnan and J. F. Stebbins, *Science* **265**, 1206 (1994); J. F. Stebbins, S. Sen, I. Farnan, *Am. Mineral.* **80**, 861 (1995).
28. G. Adam and J. Gibbs, *J. Chem. Phys.* **43**, 139 (1965); M. Goldstein, *ibid.* **51**, 3728 (1969); P. Richet, *Geochim. Cosmochim. Acta* **48**, 471 (1984); C. A. Angell, *Science* **267**, 1924 (1995).
29. J. P. Itie *et al.* *Phys. Rev. Lett.* **63**, 398 (1989); D. J. Durben and G. H. Wolf, *Phys. Rev. B* **43**, 2355 (1991); C. Meade, R. J. Hemley, H.-K. Mao, *Phys. Rev. Lett.* **69**, 1387 (1992); K. H. Smith, E. Shero, A. Chizmeshya, G. H. Wolf, *J. Chem. Phys.* **102**, 6851 (1995).
30. D. C. Rubie, C. R. Ross, M. R. Carroll, S. C. Elphick, *Am. Mineral.* **78**, 574 (1993); B. T. Poe, D. C. Rubie, P. F. McMillan, J. Diefenbacher, *Eos* **75**, 713 (1994).
31. Supported by NSF under grants DMR-9121570, CHE-9214799, and EAR-9219504. We thank K. J. Culbreath for helpful discussions and D. C. Rubie for use of the multi-anvil facility at Bayerisches Geoinstitut.

11 July 1995; accepted 16 October 1995

High-Resolution Microcoil ^1H -NMR for Mass-Limited, Nanoliter-Volume Samples

Dean L. Olson, Timothy L. Peck, Andrew G. Webb, Richard L. Magin, Jonathan V. Sweedler*

High-resolution, proton nuclear magnetic resonance (NMR) spectra of 5-nanoliter samples have been obtained with much higher mass sensitivity [signal-to-noise ratio (S/N) per micromole] than with traditional methods. Arginine and sucrose show a mean sensitivity enhancement of 130 compared to 278-microliter samples run in a 5-millimeter tube in a conventional, commercial probe. This can reduce data acquisition time by a factor of $> 16,000$ or reduce the needed sample mass by a factor of about 130. A linewidth of 0.6 hertz was achieved on a 300-megahertz spectrometer by matching the magnetic susceptibility of the medium that surrounds the detection cell to that of the copper coil. For sucrose, the limit of detection (detoured at $\text{S/N} = 3$) was 19 nanograms (56 picomoles) for a 1-minute data acquisition. This technique should prove useful with mass-limited samples and for use as a detector in capillary separations.

Compared to other common spectroscopic methods of molecular characterization, NMR is by far the least sensitive (1). NMR is seldom the method of choice for analysis of trace level quantities, despite its strong structural identification capability and non-destructive nature. In this report, we describe an NMR radiofrequency (rf) transmission/detection coil that is more than an order of magnitude smaller than typical coils (2, 3). The increase in mass sensitivity, defined as the signal-to-noise ratio (S/N) per micromole, is greater than 100-fold compared to conventional NMR. Although we previously demonstrated the feasibility of microcoil NMR spectroscopy for capillary electrophoresis (CE) and liquid chromatography (3), typical linewidths of 11 Hz were obtained, which were broad compared to conventional systems and prevented observation of proton scalar coupling. The approach reported here provides high-resolution NMR spectra by surrounding the coil region with a magnetic susceptibility matching fluid (Fig. 1). Efforts by others to improve sensitivity for NMR imaging have included the use of high-temperature superconducting coil materials and NMR force microscopy (4).

For rf coils ≤ 1 mm in diameter, the noise in an NMR experiment is dominated

by thermal noise from the coil and not the sample (5). As the coil size is reduced, the strength of the rf magnetic field per unit current increases, thereby improving mass sensitivity (6). The S/N per unit volume achieved by a solenoidal microcoil in an NMR experiment is proportional to the quantity of sample and inversely proportional to the coil diameter (6).

Fabrication of the coil shown in Fig. 2 was modified from earlier work (3, 7). The microcoil is 1 mm long and encloses a sample volume of 5 nl within the capillary [76.5 μm inside diameter and 357 μm outside diameter (OD)]. The capillary functions as both the coil form and sample container and provides a flow-through means of sample loading. The sample is not spun, and sample loading through the capillary usually makes shimming between different samples unnecessary.

Compared to previous microcoil NMR results (3), several distinct improvements were devised to obtain the high resolution reported here. Cyanoacrylate adhesive was used to hold the coil in place instead of epoxy. This adhesive readily flows into the interface between the capillary and wire coatings and allows the matching fluid to come in close proximity to the coil material. Placement of the coil at the vertical and axial center of the shims allows rapid manual and automatic shim optimization. In addition, the capillary OD was increased from 325 to 357 μm (by leaving intact the 16- μm -thick polyimide coating).

To reduce the effects of magnetic susceptibility caused by proximity of the rf coil to the sample, Fluorinert FC-43, a perflu-

D. L. Olson and J. V. Sweedler, Beckman Institute and Department of Chemistry, University of Illinois, 600 S. Mathews, Urbana, IL 61801, USA.

T. L. Peck, A. G. Webb, R. L. Magin, Magnetic Resonance Engineering Laboratory, Beckman Institute, and Department of Electrical and Computer Engineering, University of Illinois, 405 N. Mathews, Urbana, IL 61801, USA.

*To whom correspondence should be addressed.